Accepted Manuscript

Interfacial engineering of layered double hydroxide toward epoxy resin with improved fire safety and mechanical property

Zhi Li, Zhiqi Liu, Dufosse François, Luke Yan, De-Yi Wang

PII: S1359-8368(18)30764-9

DOI: 10.1016/j.compositesb.2018.08.094

Reference: JCOMB 5924

To appear in: *Composites Part B*

Received Date: 7 March 2018

Revised Date: 10 July 2018

Accepted Date: 23 August 2018

Please cite this article as: Li Z, Liu Z, François D, Yan L, Wang D-Y, Interfacial engineering of layered double hydroxide toward epoxy resin with improved fire safety and mechanical property, *Composites Part B* (2018), doi: 10.1016/j.compositesb.2018.08.094.

Graphical Abstract

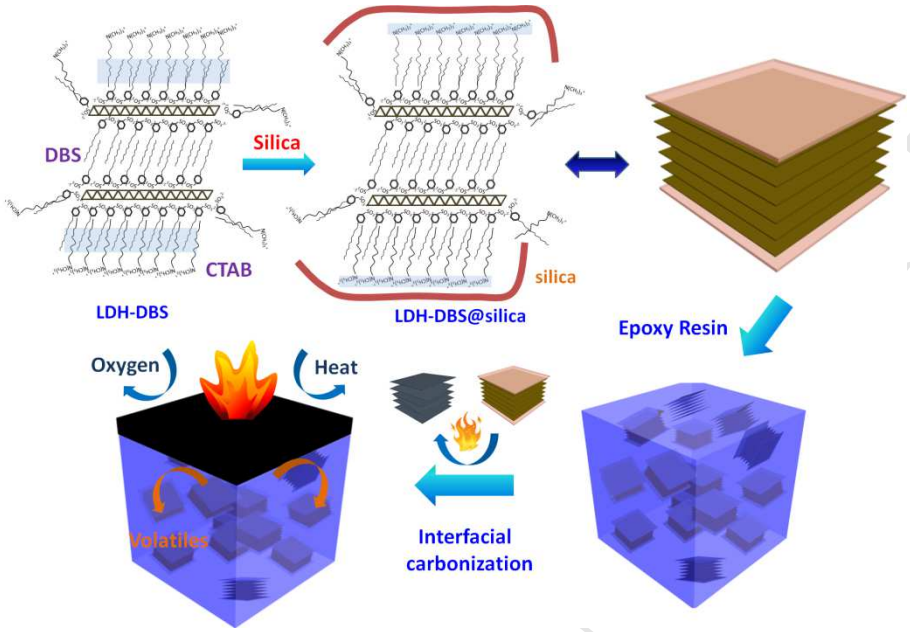

Interfacial Engineering of Layered Double Hydroxide toward Epoxy Resin with Improved Fire Safety and Mechanical Property

Zhi Li[a,b], Zhiqi Liu[a,c], Dufosse François [a], Luke Yan [d], De-Yi Wang[a*]

[a] *IMDEA Materials Insitute, C/Eric Kandel, 2, 28906 Getafe, Madrid, Spain*

[b] *Universidad Politécnica de Madrid, E.T.S. de Ingenieros de Caminos, 28040 Madrid, Spain*

[c] *Key Laboratory of Comprehensive and Highly Efficient Utilization of Salt Lake Resources, Qinghai Institute of Salt Lakes, Chinese Academy of Sciences, Xining, 810008, China*

[d]*Polymer Materials & Engineering Department,School of Materials Science & Engineering, Chang'an University, Xi 'an 710064, China*

[*]Corresponding author. Tel: +34 917871888

Email address: deyi.wang@imdea.org

Abstract

Aiming to imparting epoxy resin (EP) matrix with highly efficient fire safety and mechanical strength, the organic intercalated layered double hydroxide nanosheets (LDH-DBS) were functionalized by silica via electrostatic assembly. EP nanocomposite with resultant nanohybrid LDH-DBS@silica-1 was constructed and verified. Results showed that 3wt% LDH-DBS@silica-1 endowed EP matrix with self-extinguishment (close to V-1) in contrast to burning-to-clamp of EP/3LDH-DBS (EP with 3wt% LDH-DBS). Meanwhile, EP/3LDH-DBS@silica-1 (EP with 3wt% LDH-DBS@silica-1) possessed 63.3% and 29.2% lower peak heat release rate than EP and EP/3LDH-DBS separately, accompanied by remarkably reduced smoke and CO production. The mechanism study illustrated that the optimization of intumescent char accounted for improved fire safety due to the interfacial charring reaction toward stable cordierite ($5SiO_2 \cdot 2Al_2O_3 \cdot 2MgO$) and smaller microcrystalline carbon. The spatially preferential assembly of silica on LDH nanosheets was proposed to contribute to the dynamic char reconstruction. In parallel, LDH-DBS@silica-1 enhanced glass transition temperature of EP by 8 ^{o}C. The more silica endowed EP matrix with progressively increased non-notched impact strength. In perspective, the interfacial engineering of LDH nanosheets offered an effective approach to strengthening fire safety of polymers.

Key Words:

Polymer-matrix composites (PMCs); Layered structures; Theromosetting resin; Fire retardancy

1. Introduction

Epoxy resin (EP) incites strong interests due to superior mechanical property, low thermal shrinkage coefficient and high flexibility in choice of monomers and curing agents. Resultantly, EP enjoys extensive applications in electronic industries [1, 2] and as the matrix resin of advanced structural laminates for automotive and aircraft [3]. In certain circumstances (*e.g.*, aircraft engine), the fire hazard of structural composites poses a remarkable threat to the sustainable service due to the intrinsic flammability of the matrix EP [4, 5]. The elevated temperature from combustion damages the interface due to the thermal expansion mismatch of fibres and matrix resin. The mechanical property of EP matrix is also deteriorated in case of the occurrence of thermal degradation. Reasonably, the key to mitigating fire hazard of structural composites is to improve the fire safety of matrix resin EP [6]. In order to address the issue, various fire-retardant strategies are figured out mainly including intrinsic and additive-type phosphorous-based fire retardants [7-9] and nano-fillers [10-12]. Some phosphorus-based fire retardants possess the drawback of deteriorating thermal stability and mechanical property of matrix resin [13, 14]. In contrast, the employment of nanofillers arouses magnificent attentions attributed to notably enhanced fire safety and other comprehensive property [15, 16]. The fire-retardant mechanism involves the formation of mechanically robust barrier to restrict mass and heat transfer [17]. Actually, as far as fire tests are concerned, it is difficult to attain satisfied performance simultaneously in cone calorimeter test, LOI (limiting oxygen index) and UL-94 burning test with the mere nanoclays.

Among nano-fillers, layered double hydroxide (LDH) witnesses the enormous utilizations in EP composites. LDH possesses the typical lamellar structure with anions intercalated in the galleries with the formula $[M^{2+}_{1-x}M^{3+}_{x}(OH^{-})_2]^{x+}A^{n-}_{x/n}/n\cdot yH_2O$. Herein, M^{2+} and M^{3+} are corresponding to metal

cations with divalency and trivalency. A and n^- represented intercalating A with the valence of n^- [18]. In terms of polymer composites with LDH nanosheets, proper intercalators were generally selected to enlarge the gallery distance, aiming to enhance LDH dispersion and improve integral property. For example, dodecyl benzene sulfonate (DBS) intercalated MgAl-LDH (LDH-DBS) demonstrated a significant reinforcement of fire retardancy and mechanical property of PMMA and PS [19]. The synergistic effect and co-intercalation associated with LDH were revealed as facile approaches to reinforcing fire retardancy [20-22]. However, the previous studies illustrated that approximately 6wt% LDH derivatives were required to achieve the excellent integral fire safety [20]. The search of facile functionalization of LDH toward highly efficient integral fire safety was ongoing.

Silicon-derivations are employed as effective mono-component fire retardants or as synergistic agents based on the formation of protective carbonaceous layers [23]. Therefore, it was reasonable that LDH-DBS in combination with silica enabled to generate an excellent synergistic effect toward EP. LDH-DBS released water for flame inhibition and simultaneously promoted the formation of high-quality intumescent char. Silica was capable to react with LDH to yield Mg-O-Si and Al-O-Si structure, which favoured heat-resistant and high-strength char [24]. Herein, as the important complementation, we grew silica on the exterior surface of organic intercalated LDH via surfactant-induced in-situ sol-gel approach. The intention was to perform the function of interface-located silica between LDH and EP matrix in enhancing charring reaction toward better quality. Additionally, in consideration of relatively high elasticity of silica layers at the interface between EP and LDH-DBS, the toughening of EP composites was expected.

Aiming to significantly enhance fire safety and impact toughness of EP matrix, nanohybrid with varied loadings of silica (LDH-DBS@silica) was prepared via in-situ sol-gel technique under

electrostatic interplay. Various techniques were employed to verify the structure and component of LDH-DBS@silica. It was expected that the silica located at the interface of LDH and EP matrix facilitated the intumescent process of EP nanocomposites via the spatially preferentially charring reaction. The integral fire safety was performed using LOI test, UL-94 vertical burning test and cone calorimeter test (CCT) with focus on the fire-retardant mechanism. The char analysis in condensed phase and volatile evaluation in vapor phase were studied. Meanwhile, dynamic mechanical property and impact strength were analyzed.

2. Experimental

2.1 Materials

Tetraethyl orthosilicate (TEOS), aluminum nitrate nonahydrate ($Al(NO_3)_3 \cdot 9H_2O$), magnesium nitrate hexahydrate ($Mg(NO_3)_2 \cdot 6H_2O$), sodium hydroxide (NaOH), sodium dodecylbenzenesulfonate (SDBS), cetyltrimethyl ammonium bromide (CTAB) and aqueous ammonia ($NH_3 \cdot H_2O$) were purchased from Sigma-Aldrich without further purification. Epoxydharz C was obtained from Faserverbundwerkstoffe Composite Technology Company. 4,4'-diaminodiphenylmethane (DDS) as the curing agent was acquired by TCI EUROPA. The deionized water was produced by our institute. LDH-NO_3 was kindly supplied by Prolabin & Tefarm Company, Italy.

2.2 Preparation of silica engineering LDH-DBS (LDH-DBS@silica)

Firstly, DBS intercalated MgAl LDH (LDH-DBS) was synthesized via co-precipitation method [25]. The co-precipitation occurred when the mixed aqueous solution of 0.2M $Mg(NO_3)_2 \cdot 6H_2O$ and 0.1M $Al(NO_3)_3 \cdot 9H_2O$ were dropped to 0.1M SDBS solution with pH value adjusted at 10±0.2 by 1M NaOH solution. The final product (LDH-DBS) was acquired after the filtration, washing and drying treatment. The weight fraction of DBS reached 56.6% in LDH-DBS characteried by Element Analysis. In parallel,

the preparation of LDH-DBS@silica was conducted through sol-gel technique under structure-directing agent (CTAB) (**Scheme 1**). In detail, 10g dry LDH-DBS was dispersed in mixed solution of ethanol (200mL) and deionized water (389 mL) homogeneously under ultrasonication in 1L signal-neck flask. 1.22g CTAB was then dissolved in the suspension with vigorous stirring, followed by adding 2.2mL aqueous ammonia. Subsequently, 200mL aqueous solution with 0.81g TEOS was dropwise added to the above system, followed by 3h reaction. Subsequently, the stirring velocity was adapted to slightly weaker and the reaction proceeded for another 3h. After the reaction ended, the product was filtrated and washed for 3 times with hot water. The air-drying procedure was applied at 80^{o}C overnight to obtain the product LDH-DBS@silica. Herein, the polycondensation degree of TEOS was regarded as about 50% according to calculation in the literature [26]. In this case, the obtained nanohybrid LDH-DBS@silica contained 2wt% of silica, thus donated as LDH-DBS@silica-2. In parallel, LDH-DBS@silica-0.5, LDH-DBS@silica-1, LDH-DBS@silica-2 and LDH-DBS@silica-4 were separately prepared. LDH-DBS@silica donated the category of DBS-LDH hybrid with silica modification.

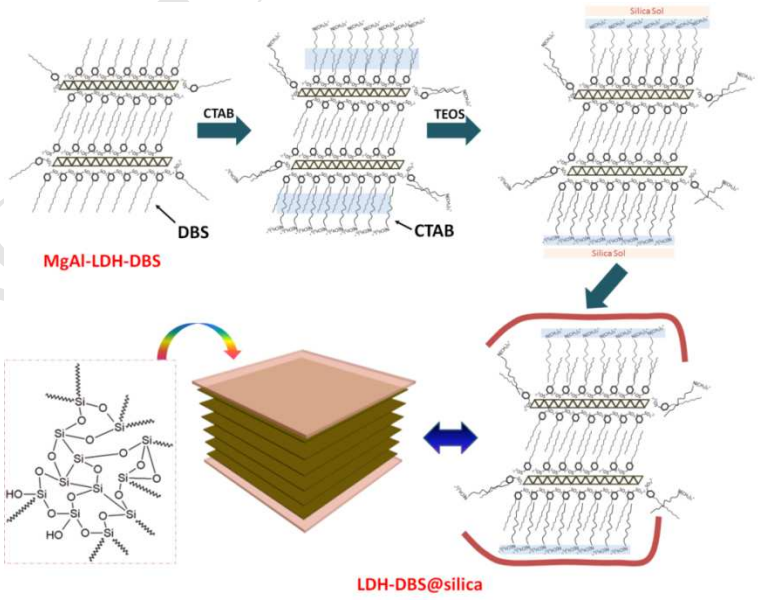

Scheme 1 Preparation process of LDH-DBS@silica

2.3 Fabrication of EP and EP composites

EP composites with 3wt% LDH-DBS, LDH-NO_3 and LDH-DBS@silica were fabricated respectively. In detail, EP monomer and 3wt% fillers were mixed at 50^{o}C to get preliminary dispersion. After that, the triple milling machine was employed to further disperse LDH nanosheets. The resultant suspension was heated to 125^{o}C and DDS was added under vigorous stirring. Once DDS powder was completely dissolved, the system was degassed for 5min at 110^{o}C. Subsequently, the suspension was casted into silicon mould at 160^{o}C, where the primary curing reaction proceeded for 1h. Afterwards, the temperature was adjusted to 180^{o}C for 2h curing and 200^{o}C for another 1h deep curing. The prepared samples were labelled as EP/3LDH-DBS, EP/3LDH-NO_3, EP/3LDH-DBS@silica-0.5, EP/3LDH-DBS@silica-1, EP/3LDH-DBS@silica-2 and EP/3LDH-DBS@silica-4. In terms of pristine EP and EP/3SDBS (EP composite with 3wt% SDBS), the preparation followed identical procedure.

2.4 Instrumental

Raman spectra were recorded on Renishaw PLC with a Leica DM2700 microscopy. X-ray diffraction (XRD) was carried out on XPERT-PRO diffractometer facilitated with Cu Kα X-ray resource (λ=0.1542nm) and Ni filter. Scanning electron microscopy (SEM) was performed on EVO MA15, Zeiss. Field-emission scanning electron microscope (FESEM) was executed on Helios NanoLab 600i. The sample was coated with conductive gold film prior to observation. Transmission electron microscopy (TEM) was operated on Tecnai T20 (FEI Company and Talos F200X, FEI) under 200kV. As for nanocomposite, the ultrathin section was prepared using Leica ultramicrotomy diamond knife at ambient temperature. N_2 sorption was conducted with Micromeritics ASAP 2010 surface area and pore size analyzer. BET (Brunauer-Emmett-Teller) calculation of nitrogen isotherms at -196^{o}C was used to

confirm specific surface size. Pore size was determined using BJH (Barrett-Joyner-Halenda) formula. Pore volume was obtained at the relative pressure (P/P_0) of 0.98. Thermogravimetric analysis (TG) was performed on Q50 (TA Instruments) from ambient temperature to 800^{o}C at heating rate of 10^{o}C/min at N_2 and air atmosphere. The samples weight was 15±0.5mg and 5±0.2mg as to N_2 and air atmosphere respectively. Thermogravimetric analysis (Q50) coupled with Fourier transformation infrared spectra (Nicolet iS50) (TG-FTIR) was performed. The constant weight (15±0.5mg) sample was heated to 800^{o}C at 10^{o}C/min. Limiting oxygen index (LOI) was performed on LOI instrument (FTT, UK) according to ASTM D 2863-2013. UL-94 vertical burning test was analyzed using the instrument (FTT, UK) according to ASTM D 3801-2010. Cone calorimeter test (CCT) was conducted on instrument (Fire Testing Technology, UK) according to ISO 5660-1 with sample of 100×100×4 mm^3 at 50kW/m^2. As for each sample, at least 2 replicas were tested for data collection. Dynamic mechanical behavior was analyzed on dynamic mechanical analyzer (DMA, Q800, TA instruments) on single cantilever. The measurement proceeded with temperature rising from room temperature to 270^{o}C at 3^{o}C/min at the amplitude of 3μm. Impact behavior was analyzed using the impact tester (Zorn Standal, Germany) confronting to DIN 53753. The unnotched sample with 50×6×4 mm^3 was tested. The parameters of at least five samples were averaged for the final results. The samples for fire and mechanical tests were conditioned at 25^{o}C, 50% humidity for 96 h prior to experiment.

3. Results and discussions

3.1 Characterization of LDH-DBS@silica

XRD pattern

XRD patterns of LDH-DBS and LDH-DBS@silica were showed in **Fig.1** and **Fig S1**. After the incorporation of silica, XRD reflections of LDH-DBS were completely remained with identical peak

location to those of LDH@DBS (**Fig.1** (a)) [25]. The first reflection emerged at 3.0°, which indicated that the gallery spacing of (003) was 2.96nm according to Braggs' Equation. The same situation was also present in 0.5wt%, 2wt% and 4wt% silica functionalization (**Fig S1**). According to our design, during the preparation of LDH-DBS@silica, the surfactant CTAB acted as the bridge that connected the silica sol and LDH nanosheets through the non-covalent interaction with LDH-DBS and electrostatic interplay with silica sol respectively. As the silica precursor underwent sol-gel process on LDH nanosheet surfaces, the force of contraction was generated around LDH nanosheets. However, LDH-DBS was strong enough to resist the contraction effect of silica. During the functionalization, the crystallite size of LDH nanosheets did not change notably based on Scherrer Equation, which indicated silica engineering did not destroy the LDH structure.

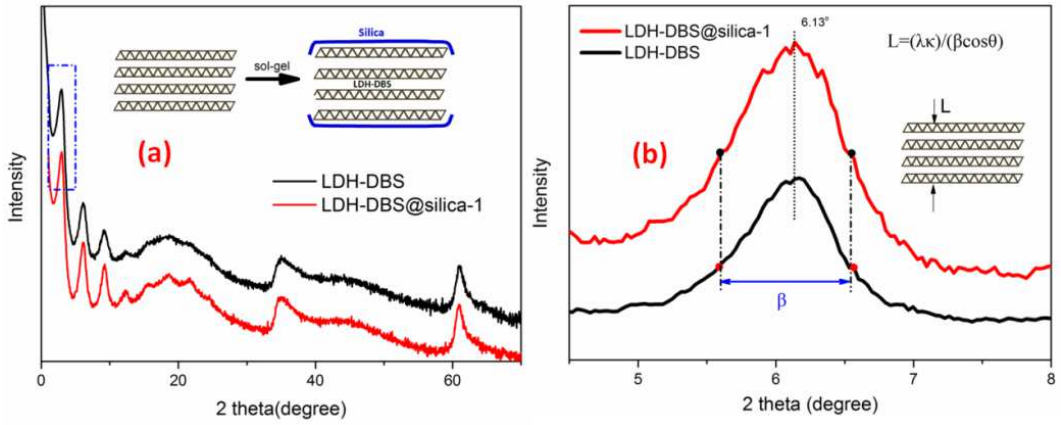

Fig.1. XRD patterns (a) at 0.2°-70° and (b) at 4°-8° of LDH-DBS and LDH-DBS@silica-1 (κ: a fixed factor; β: peak width at half-maximum height)

SEM

The morphology investigation was shown in **Fig S2**. In contrast to the aggregation state with lamellar structure of LDH-DBS (**Fig S2** (a, b)), **Fig S2** (c, d) revealed that LDH nanosheets were coated with silica remarkably (red circle), accompanied by the edges of neighboring LDH nanosheets forming the

curled orientation due to the limited space. Meanwhile, the curled orientation further manifested that the force of contraction was generated during the in-situ sol-gel process, which was in good agreement with our design. LDH nanosheets with silica coated exhibited the thickness of ca.30nm.

TEM and EDS

TEM and EDS result was revealed in **Fig.2** and **Fig S3**. In terms of LDH-DBS in **Fig.2** (a) and (b), the typical lamellar structure was observed with the aggregation state. In **Fig.2** (c) and (d), the obvious sheet-like accumulation was also detected in LDH- DBS@silica-1. Besides, thin layers of silica were present and covering LDH nanosheets along the edges. Actually, not all edges of LDH nanosheets were coated with silica, which offered the possibility of intercalation or exfoliation of LDH sheets in composites fabrications. Between silica layers and LDH nanosheets, notable void was visible, which was attributed to the surfactant CTAB. Hence, it was reasonable that the CTAB induced the in-situ coating process on LDH-DBS through electrostatic interaction. In parallel, the TEM analysis of LDH-DBS@silica-0.5 and LDH-DBS@silica-2 showed the similar result (**Fig S3**). The EDS spectra revealed the presence of Al, Mg Si, O, N and S, which belonged to DBS-LDH, silica and CTAB. The ratio of atomic percentage of Mg and Al was 2.2, very close to the feeding ratio of 2. Meanwhile, the Si elements made up 2.3% in the studied elements. Moreover, the EDS mapping (f, g, h, i and j) revealed the homogenous dispersion of Si, N, S, Mg and Al around LDH-DBS. It was noted that the combination image (**Fig.2** (e)) of HAADF and Si and N mapping at the short scanning time illustrated that silica and CTAB were coating LDH-DBS uniformly.

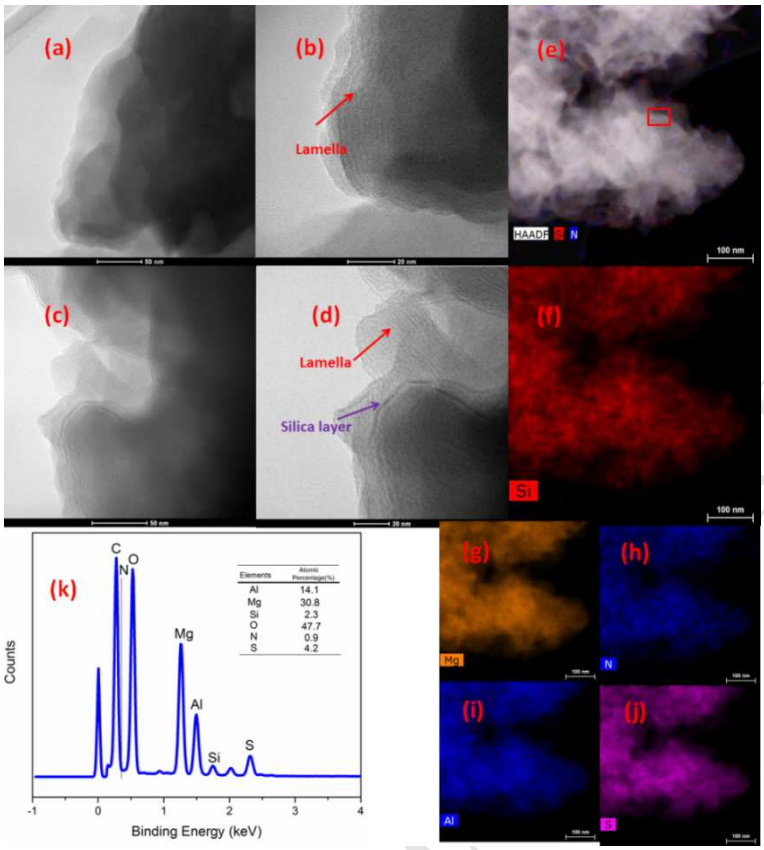

Fig.2. TEM images of (a, b) LDH-DBS and (c, d) LDH-DBS@silica-1 at different magnification; (e) High angle angular dark field (HAADF) with Si and Mg mapping at short scanning time; EDS full mapping of (f) Si, (g) Mg, (h) N, (i) Al and (j) S; (k)EDS spectra of selected area in (e) and element percentage

N_2 adsorption and desorption

In order to further investigate the coating behavior of silica on LDH-DBS, the pore property was analyzed (**Fig.3** (a)). LDH-DBS possessed the high specific surface area of 11.6m^2/g according to BET method and the large pore volume of 0.047mL/g based on the adsorption volume of N_2 at relative pressure of 0.99. The comparison of LDH-DBS, LDH-DBS@silica-0.5 and LDH-DBS@silica-1 demonstrated that the addition of 0.5wt% and 1wt% silica did not notably change the pore volume and specific surface area. As 2wt% silica was incorporated, the specific surface area and pore volume were both increased remarkably with the specific surface area of 45.3m^2/g and pore volume of 0.348mL/g.

Reasonably, the excessive incorporation of silica precursor gave rise to the mesoporous silica directed by surfactant CTAB [11]. Therefore, the disorder-to-order transition of silica was considered to occur at the loading of ca. 2wt% in the coating process.

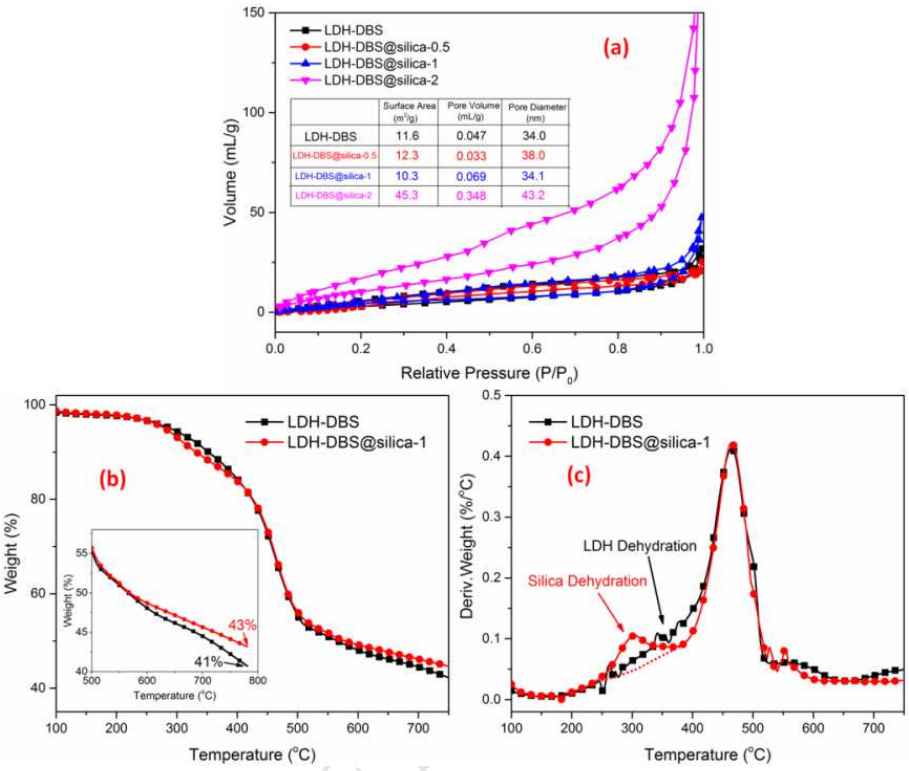

Fig.3. (a) N_2 adsorption and desorption curves of LDH-DBS and LDH-DBS@silica; (b) TG and (c) DTG curves of LDH-DBS and LDH-DBS@silica-1

Thermal degradation behavior

The thermal degradation behavior was exhibited in **Fig.3** (b) and (c). In **Fig.3** (b), LDH-DBS@silica-1 revealed higher char yield of 43wt% compared to 41wt% of LDH-DBS. The theoretical calculation toward the char yield at 680°C of LDH-DBS, LDH-DBS@silica-1 and silica [27] revealed that the silica amount was ca. 20wt%. The remarkably higher silica amount relative to EDS results indicated that silica incorporation promoted the char production. Between 250°C and 400°C, LDH-DBS@silica-1 preserved slightly lower weight than that of LDH-DBS, which was due to the dehydration of silica. In

Fig.3 (c), DBS-LDH demonstrated the maximum degradation peak located at ca 460^{o}C, which was due to the dehydration of the chemically absorbed water. When LDH-DBS was coated with silica, the dehydration of LDH-DBS did not change without visible alteration of the intensity of peak at ca 460^{o}C, which implied that the silica did not affect the dehydration.

3.2 Dispersion state of LDH-DBS@silica in EP

In order to analyze the dispersion state of LDH-DBS@silica-1 in EP, XRD and TEM were performed and showed in **Fig.4**. In **Fig.4** (a) and (d), EP matrix entered the LDH gallery to enlarge the distance from 2.96nm (LDH-DBS) to 3.42nm (EP/3LDH-DBS), which formed the intercalated polymer nanocomposite [10]. The addition of 3wt% LDH-DBS@silica-1 also obtained the intercalated EP nanocomposite. The first reflection of EP/3LDH-DBS@silica-1 shifted to lower position (gallery spacing 3.45nm) compared to EP/3LDH@DBS, which manifested that the incorporation of silica slightly promoted the intercalation process of EP molecules into LDH gallery (**Scheme S1**). In contrast, the addition of 3wt% LDH-NO_3 did not obtain the intercalated structure (**Fig S4**). TEM observation (**Fig.4** (b) and (c)) of EP/3LDH-DBS illustrated that the LDH-DBS particle was persisted in EP matrix with the exception of the formation of exfoliation structure of edge of LDH nanosheet due to the ease of EP penetration into the gallery. In **Fig.4** (e) and (f), the integral structure of EP/3LDH-DBS@silica-1 tended to become loose with EP matrix penetrated inside. The high magnification image of the edge of LDH nanosheet evidenced the intercalated structure with the gallery spacing about ca. 3.5 nm. In addition, the selected area electron diffraction (SEAD) pattern of EP/3LDH-DBS@silica-1 showed less distinct diffraction rings than that of EP/3LDH-DBS.

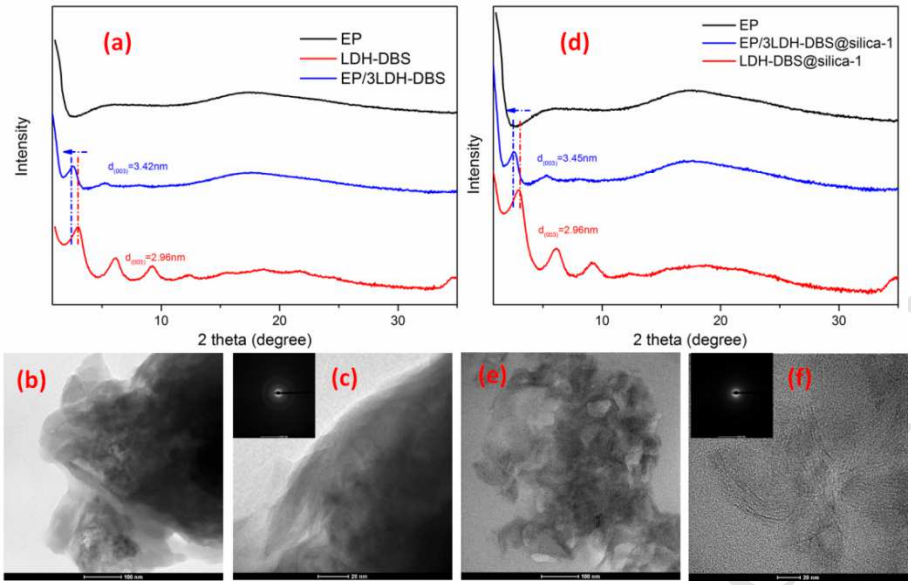

Fig.4. XRD patterns of (a) LDH-DBS and EP/3LDH-DBS and (b) LDH-DBS@silica-1 and EP/3LDH-DBS@silica-1; TEM images of (b, c) EP/3LDH-DBS

3.3 Thermal stability investigation

The thermal stability was shown in **Table S1**, **Fig S5**, **Fig S6** and **Fig.5**. The intercalation of DBS into LDH interlayers changed the main degradation peak from roughly 150°C of LDH-NO_3 to 450°C of LDH-DBS (**Fig S5**), which was attributed to the transition from the dehydration of LDH lamellas (LDH-NO_3) to DBS degradation (LDH-DBS) [28]. In contrast, the incorporation of LDH-DBS and LDH-DBS@silica reduced the initial thermal stability ($T_{5wt\%}$) of EP matrix to some degree compared with nearly no impact of LDH-NO_3 (**Fig.5**). The probable reason was due to the degradation-promoting effect of DBS (**Fig S6**) and catalyzing degradation of LDH lamellas by LDH lamellas toward EP matrix [29, 30]. The comparison of EP/3LDH-DBS and EP/3LDH-DBS@silica revealed that the silica modification slightly increased $T_{5wt\%}$ with the maximum increment of 5°C in terms of LDH-DBS@silica-4 [31]. It indicated that the silica modification was capable to resist the influence of LDH-DBS on the initial thermal degradation [32, 33]. The similar case was also shown in T_{max}. The char analysis demonstrated that LDH-DBS decreased the char percentage compared to those of

EP/3LDH-NO_3 and neat EP, which was due to the deterioration effect of DBS. However, the char yield of EP/3LDH-DBS was not affected notably with the nano-coating of silica, accompanied with the trend of the slight increase of char yield. DTG curves in **Fig.5** (b) revealed that the addition of LDH-DBS and LDH-DBS@silica showed the trend of reduction in the maximum degradation rate (R_{max}) relative to EP and EP/3LDH-NO_3 due to the formation of intercalated structure. In contrast, the silica modification did not impact R_{max} visibly compared to that of EP/3LDHH-DBS. The inconspicuous changes in $T_{5wt\%}$, T_{max}, R_{max} and char yield after the incorporation of silica was considered strongly to be associated with the low loading of silica in EP nanocomposites.

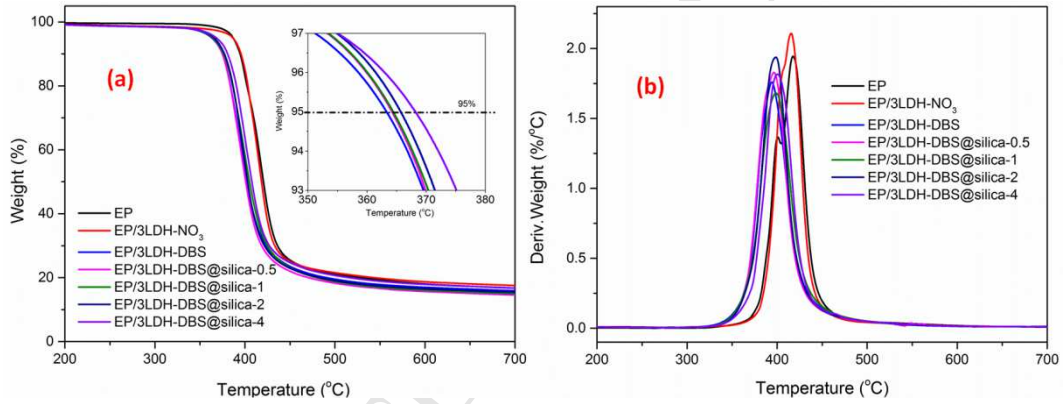

Fig.5. (a) TG and (b) DTG curves of EP and EP nanocomposite

3.4 Fire safety investigation

LOI and UL-94

LOI and UL-94 result were shown in **Table S2**. In terms of LOI, the addition of 3wt% LDH-NO_3 and LDH-DBS separately increased LOI value to 23.4% and 24.8% from 23.2% of neat EP. Silica nano-coating of LDH-DBS changed LOI values of EP nanocomposites at a nearly invisible degree, which was probably due to the fact that the low loading of silica failed to generated the high-quality char in low heat feedback condition (LOI burning mode). In contrast, in UL-94 vertical burning test,

EP, EP/3LDH-DBS and EP/3LDH-NO_3 burned to clamp, which illuminated that LDH-NO_3 and LDH-DBS was not capable to impart EP with self-extinguishing at first 10s flaming. Interestingly, after the silica modification, the EP nanocomposites self-extinguished after first 10s with the least average combustion time of 3s (EP/3LDH-DBS@silica-1). After the second 10s flaming, EP nanocomposites with silica functional LDH-DBS burned to clamp with the exception of EP/3LDH-DBS@silica-1, which self-extinguished at average combustion time of 27s. In consideration of UL-94 standard about the addition value of first and second combustion time of each sample, EP/3LDH-DBS@silica-1 was not classified as V-1 but as the self-extinguishing type. In the similar studies, the self-extinguishment was attained with 5wt% [10] or 6wt% [20] functionally intercalated LDH, which was higher than 3wt% of the present research. Herein, the divergence of UL-94 and LOI was due to the inclination of these two tests. LOI focused on ignitability and UL-94 stressed on the resistance of fire spreading (relatively higher heat feedback) [34].

Cone calorimeter test

EP, EP/3LDH-NO_3, EP/3LDH-DBS and EP/3LDH-DBS@silica-1 were selected to perform the CCT test in consideration of best UL-94 performance of EP/3LDH-DBS@silica-1 in LDH-DBS@silica filled EP composites. In **Fig.6** (a) and **Table 1**, the addition of 3wt% LDH-NO_3 and LDH-DBS decreased pHRR value of EP to certain degrees. Remarkably, EP/3LDH-DBS@silica-1 possessed pHRR of 355±8 kW/m^2, 63.3% and 29.2% lower than EP and EP/3LDH-DBS separately, which indicated that silica incorporation reduced the fire intensity notably. The reduction of pHRR value was comparable to EP nanocomposites with 5wt% and 6wt% functionally intercalated LDH (62% [10] and 66% [20] reduction respectively). In terms of the combustion period that was marked within the dotted ellipsoid, the char reconstruction proceeded after the char fracture. It was reasonably defined that the sloop of the period embodied the difficulty of char reconstruction. The sloop followed the sequence: $k_{EP/3LDH\text{-}DBS@silica\text{-}1} < k_{EP/3LDH\text{-}DBS} < k_{EP/3LDH\text{-}NO3} < k_{EP}$, which indicated that silica improved the char reconstruction and thus protected the underlying matrix from further oxygen and heat. Meanwhile,

the high HRR value of EP/3LDH-DBS@silica-1 remained until 500s, which was different from those of EP and other EP composites. The result illustrated that the formed carbonaceous layers at 300s underwent further combustion at very low fire intensity. It was notable that the silica percentage in EP/3LDH-DBS@silica-1 was calculated as 0.03%, which was much lower than the reported loading as the synergistic agents [35]. The probable reason was due to the direct nanocoating of silica on LDH nanosheets favored the synergetic chemical reaction remarkably. In addition, THR value at 200s of EP/3LDH@silica-1 was 26.2±1.9MJ/m^2, which was 63.3% and 50.1% lower than those of neat EP and EP/3LDH-DBS respectively. The combustion intensity was also reflected in AMLR (**Fig S7** (a) and **Table 1**) and FIGRA, which focused separately on mass loss and fire growth profile. EP/3LDH-DBS@silica-1 possessed the AMLR of 0.057±0.001 g/s and FIGRA of 1.15 kW/(m^2·s), which were 27.8% and 54.4% lower than those of EP/3LDH-DBS@silica-1.

The fire hazard was also evaluated by toxic gases and smoke (**Fig.6** (d) and **Fig S7** (b, c, d)). Herein, TSP at 200s of EP/3LDH-DBS@silica-1 was reduced by 64.0% and 48.1% respectively compared with EP and EP/3LDH-DBS. The peak smoke production rate was also remarkably reduced after modification of silica. Interestingly, the ratio of COP and CO2P was delayed notably in terms of EP/3LDH-DBS@silica-1 in comparison to those of EP/3LDH-NO_3 and EP/3LDH-DBS., which illustrated that the occurrence of the toxicity was delayed. In parallel, the comprehensive efficient heat of combustion (EHC) herein was obtained as THR divided by TML. During the first 200s, the addition of 3wt% LDH-NO_3 imparted EP with EHC of 2.24±0.01 MJ/(m^2·g), lower than that of neat EP (2.55±0.01 MJ/(m^2·g)), which illuminated that the vapor fire retardant mechanism was present especially in the early stage of combustion. The vapor mechanism became weaker in EP/3LDH-DBS and EP/3LDH-DBS@silica based on the higher EHC value in contrast to that of EP/3LDH-NO_3.

Table 1 CCT data of EP and EP composites (50kW/m^2)

Sample	pHRR (kW/m^2)	THR (MJ/m^2) at 200s	TSP (m^2) at 200s	AMLR (g/s)	FIGRA (kW/(m^2·s))	THR/TML (MJ/(m^2·g)) at 200s
EP	967±45	71.4±3.4	22.5±0.5	0.110±0.009	6.03	2.55±0.01
EP/3LDH-NO_3	730±32	58.5±3.1	19.2±1.3	0.100±0.008	3.73	2.24±0.01
EP/3LDH-DBS	502±21	52.5±2.9	15.6±1.0	0.079±0.006	2.52	2.51±0.01
EP/3LDH-DBS@silica-1	355±8	26.2±1.9	8.1±0.5	0.057±0.001	1.15	2.47±0.01

pHRR: Peak heat release rate THR at 200s : Total heat release at 200s TSP: Total smoke production AMLR: Average mass loss rate TML: Total mass loss FIRGA: Fire growth rate

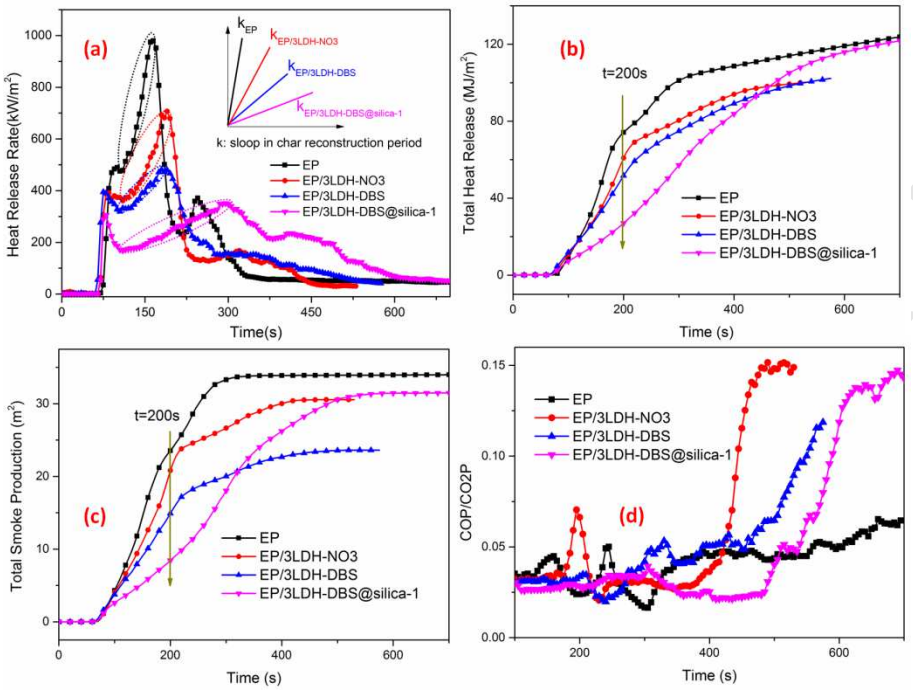

Fig.6. (a) HRR, (b) THR, (c) TSP and (d) COP/CO_2P value of EP and EP nanocomposites

Char analysis

The char structure after CCT was investigated by digital image, SEM and Raman spectra (**Fig.7** and **Fig S8**). The comparison of digital images of EP and EP composites demonstrated that the silica encapsulation imparted EP with more compact and intumescent char structure, which favored the barrier of heat, oxygen and fuel supply. The SEM analysis of char disclosed that the more continuous interior surface of EP/3LDH-DBS@silica-1 was generated with less cracks and holes compared with those of EP and EP/3LDH-DBS. Meanwhile, the char of EP/3LDH-DBS@silica-1 became flockier, which evidenced that the carbonaceous layer turned more robust to form intumescent structure. XRD analysis of char from EP/3LDH-DBS@silica-1 illustrated that Si element of silica reacted with Mg and Al element of LDH to form cordierite ($5SiO_2 \cdot 2Al_2O_3 \cdot 2MgO$), which further favored the formation of structurally-stable protective char during combustion (**Fig S9**) [36]. Moreover, the neighboring locations of LDH and silica in EP matrix favored the reaction remarkably. Raman spectra analysis revealed the presence of D peak (ca. 1356cm^{-1}) and G peak (ca. 1588cm^{-1}), which were respectively attributed to A_{1g} breathing vibration of sp3 hybridized carbon and E_{2g} in-plane stretching of six-ring

sp2 carbon [37]. The peak intensity ratio of D and G band (ID/IG) reflected the micro-crystallite size of carbon. ID/IG value of EP composites did not showed notable difference with the value of EP/3LDH-DBS@silica-1 slightly higher. It indicated that in the char of the studied EP composites, EP/3LDH-DBS@silica-1 possessed slightly smaller crystallite size and better char quality [38]. Conclusively, the silica modification promoted the enhancement of char quality of EP composite.

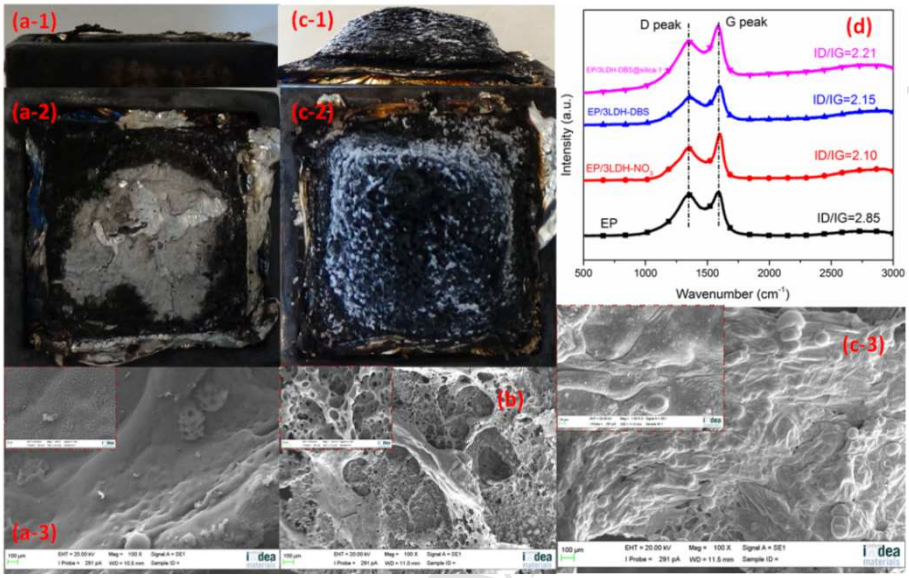

Fig.7 (a-1) Lateral and (a-2) top view of EP; (c-1) lateral and (c-2) top view of EP/3LDH-DBS@silica-1; SEM image of interior surface of (a-3) EP, (b) EP/3LDH-DBS and (c)EP/3LDH-DBS@silica-1; (d) Raman spectra of EP and EP composites

Fire-retardant mechanism

Based on comprehensive analysis, the fire-retardant mechanism of EP/3LDH-DBS@silica was involved predominantly in the condensed phase and secondarily in vapor phase (**Scheme 2**). TG result of LDH-DBS@silica-1 showed that the water release behavior occurred at 290^{o}C and 460^{o}C. The vapor-phase mechanism from cooling of combustion zone was present, which was evidenced by the slight reduction of comprehensive EHC. Furthermore, the highly intumescent char with compact interior structure was generated, accompanied by the formation of stable cordierite ($5SiO_2 \cdot 2Al_2O_3 \cdot 2MgO$) and smaller microcrystalline carbon. In detail, EP matrix decomposed and generated char at 460^{o}C (**Fig.5**), resulting in the formation of dehydrated LDH reinforced carbonaceous layer. The further increasing temperature gave rise to the chemical dehydration of LDH nanosheets toward layered double oxide (LDO), accompanied by the charring reaction of EP. As a result, the

intumescent char structure with LDO reinforcing component was accordingly generated. Reasonably, the intercalated LDH structure in EP matrix played a key role in the formation of intumescent char. Particularly, the incorporation of silica at the interface between LDH and EP matrix resulted in the formation of stable cordierite ($5SiO_2 \cdot 2Al_2O_3 \cdot 2MgO$) via the reaction of silica and LDH. The smaller microcrystalline carbon from the decomposition of EP matrix was induced probably due to the presence of stable cordierite. From another aspect, the spatially preferential silica was capable to promote the charring reaction of EP matrix [11], which resulted in the strengthened char structure. The intumescent char acted as the excellent barrier of heat, oxygen and flammable volatiles [14, 39]. Actually, after the incorporation of silica, the volatile specimens did not reveal the notable alteration (**Fig S10**), which indicated that silica exerted the main effect in participating in the charring but not changed the degradation route.

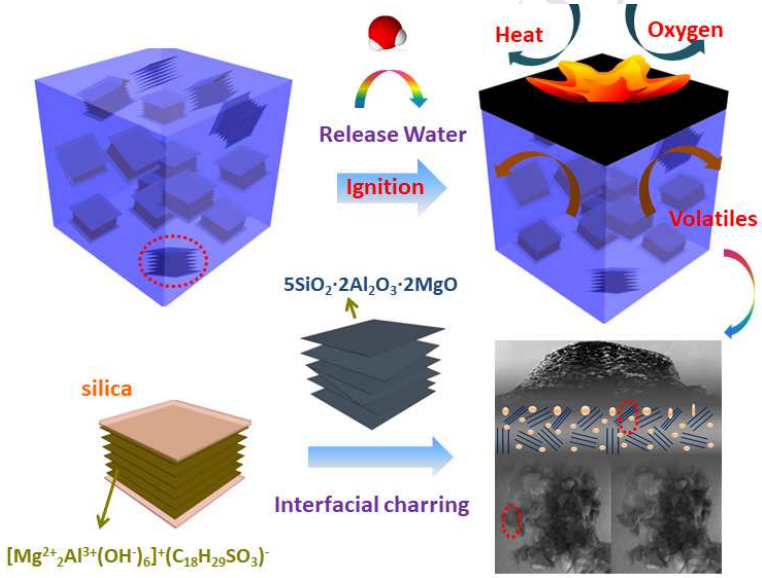

Scheme 2 Fire-retardant mechanism of EP/3LDH-DBS@silica-1

3.5 Dynamic mechanical behavior and impact behavior

Dynamic mechanical property and impact strength of EP and EP composites were exhibited in **Fig.8**. In **Fig.8** (a) and (b), the addition of LDH-DBS and LDH-DBS@silica collectively increased the storage modulus (G') of EP to varied degrees with EP/3LDH-DBS@silica-4 highest increment of 27.5%. In contrast to EP/3LDH-DBS, EP/3LDH-DBS@silica did not reveal notable alteration, which was

possibly due to the maintenance of the interaction between nanofillers and EP. In parallel, the glass transition temperature (T_g) of EP was increased with the addition of LDH-DBS and LDH-DBS@silica with the maximum T_g (210^{o}C) of EP/3LDH-DBS@silica-1 (**Table S3**). Reasonably, the increase of T_g was originated from formation of the intercalation structure, which further restricted the movement of EP segments [35]. EP/3LDH-DBS@silica-4 possessed the exclusive T_g value of 198^{o}C, lower than that of neat EP (202^{o}C). According to the result from N_2 sorption, LDH-DBS@silica-4 possessed excessive silica, which formed the mesopores structure. Therefore, it was understandable that EP/3LDH-DBS@silica-4 possibly possessed weaker intercalation structure, which account for the reduction of T_g. The excessive silica in EP composites resulted in the increased plasticizing effect [40], which also induced the drop of T_g.

Non-notched impact result was showed in **Fig.8**. After the addition of 3wt% LDH-DBS, the impact strength was reduced to 4.8±0.7 KJ/m^2 from 9.2±2.1 KJ/m^2 of EP, which was in agreement of the morphology of EP/3LDH-DBS disclosed in TEM. Even though the intercalation structure was formed, the aggregation state was notable and thus the crack tended to be initiated. After the silica incorporation, the impact strength increased gradually with more loading of silica. EP/3LDH-DBS@silica-4 demonstrated more impact strength (10.3±1.7 KJ/m^2) than that of neat EP and other EP composites. The image analysis revealed the generation of whitening at the fracture zone, which manifested that the craze occurred with the addition of silica (**Fig.8** (e)). Herein, LDH-DBS@silica-4 formed the core-shell with the rigid LDH nanosheets and micrometric soft silica layers, which favored the formation of craze (**Fig.8 (d)**) [41]. In detail, the silica nano-layer actually tended to initiate the local generation of shear band at interface, which further induced the formation of enormous craze (stress whitening). Meanwhile, the debonding occurring at the interface also dissipated the impact energy effectively [42].

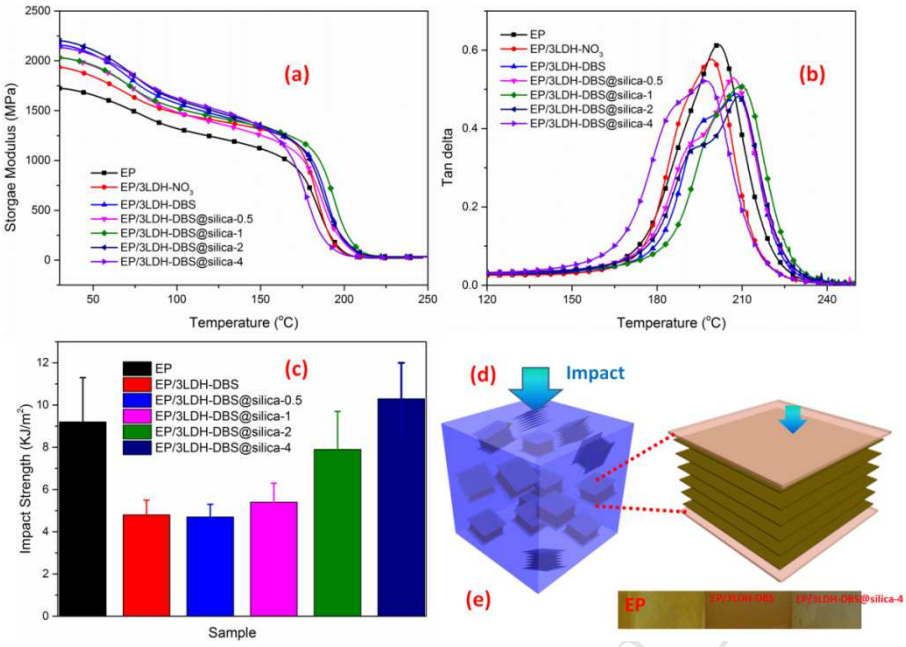

Fig.8. (a) Storage modulus and (b) tan delta of EP and EP composites; (c) Non-notched impact strength of EP and EP composites; (d) schematic illustration of possible energy dissipation with the inset facture surface of EP, EP/3LDH-DBS and EP/3LDH-DBS@silica-4

4. Conclusion

In the article, DBS intercalated LDH nanosheets were interfacially engineered by silica gel via electrostatic self-assembly and in-situ sol-gel approach. The intercalation nanostructure of resultant EP/3LDH-DBS@silica-1 in EP matrix was verified. The thermal stability of EP matrix was enhanced with the incorporation of silica. 3wt% LDH-DBS@silica-1 endowed EP with self-extinguishment property (close to V-1), accompanied by notably decreased heat release (63.3% reduction in pHRR), smoke and CO production. The mechanism analysis illustrated that the optimization of intumescent char structure toward the formation of stable cordierite and less crystalline-size char accounted for the improved fire safety. In the mesoscale, the interfacial location of silica between LDH nanosheets and EP matrix was proposed to promote the optimization of microstructure via participating in the charring reaction. The more silica encapsulation of LDH-DBS gradually increased non-notched impact strength.

In perspective, the interfacial engineering of silica on LDH nanosheets offered a highly effective approach to strengthening fire safety of polymers.

Acknowledgements

This research is funded by Spanish Ministry of Economy and Competitiveness (MINECO) under Ramón y Cajal fellowship (RYC-2012-10737), COST Action CM1302 (Smart Inorganic Polymers), Science and Technology of Qinghai Program (No.2015-HZ-812) and Natural Science Foundation of China (No.U1607104).

References

[1] Liu S, Chevali VS, Xu Z, Hui D, Wang H. A review of extending performance of epoxy resins using carbon nanomaterials. Composites Part B: Engineering. 2017.

[2] Li Z, Liu L, González AJ, Wang D-Y. Bioinspired polydopamine-induced assembly of ultrafine $Fe(OH)_3$ nanoparticles on halloysite toward highly efficient fire retardancy of epoxy resin via an action of interfacial catalysis. Polymer Chemistry. 2017;8(26):3926-36.

[3] Phonthammachai N, Li X, Wong S, Chia H, Tjiu WW, He C. Fabrication of CFRP from high performance clay/epoxy nanocomposite: Preparation conditions, thermal-mechanical properties and interlaminar fracture characteristics. Composites Part A: Applied Science and Manufacturing. 2011;42(8):881-7.

[4] Tranchard P, Samyn F, Duquesne S, Estèbe B, Bourbigot S. Modelling behaviour of a carbon epoxy composite exposed to fire: Part I-Characterisation of thermophysical properties. Materials. 2017;10(5):494.

[5] Qian L, Qiu Y, Wang J, Xi W. High-performance flame retardancy by char-cage hindering and free radical quenching effects in epoxy thermosets. Polymer. 2015;68:262-9.

[6] Zhao X, Yang L, Martin FH, Zhang X-Q, Wang R, Wang D-Y. Influence of phenylphosphonate based flame retardant on epoxy/glass fiber reinforced composites (GRE): Flammability, mechanical and thermal stability properties. Composites Part B: Engineering. 2017;110:511-9.

[7] Zhang W, Fina A, Cuttica F, Camino G, Yang R. Blowing-out effect in flame retarding epoxy resins: Insight by temperature measurements during forced combustion. Polym Degrad Stabil. 2016;131:82-90.

[8] Velencoso MM, Battig A, Markwart JC, Schartel B, Wurm FR. Molecular Firefighting□How Modern Phosphorus Chemistry Can Help Solve the Flame Retardancy Task. Angewandte Chemie. 2018.

[9] Xu Y-J, Wang J, Tan Y, Qi M, Chen L, Wang Y-Z. A novel and feasible approach for one-pack flame-retardant epoxy resin with long pot life and fast curing. Chem Eng J. 2018;337:30-9.

[10] Das A, Wang D-Y, Stockelhuber KW, Jurk, R, Fritzsche J, Kluppel M, Heinrich G. Rubber-Clay Nanocomposites: Some Recent Results. Advances in Polymer Science. 2011; 239:85-166.

[11] Li Z, González AJ, Heeralal VB, Wang D-Y. Covalent assembly of MCM-41 nanospheres on graphene oxide for improving fire retardancy and mechanical property of epoxy resin. Composites Part B: Engineering. 2018;138:101-12.

[12] Raimondo M, Guadagno L, Speranza V, Bonnaud L, Dubois P, Lafdi K. Multifunctional graphene/POSS epoxy resin tailored for aircraft lightning strike protection. Composites Part B: Engineering. 2018;140:44-56.

[13] Jing J, Zhang Y, Tang X, Zhou Y, Li X, Kandola BK, et al. Layer by layer deposition of polyethylenimine and bio-based polyphosphate on ammonium polyphosphate: A novel hybrid for

simultaneously improving the flame retardancy and toughness of polylactic acid. Polymer. 2017;108:361-71.

[14] Khalili P, Tshai K, Hui D, Kong I. Synergistic of ammonium polyphosphate and alumina trihydrate as fire retardants for natural fiber reinforced epoxy composite. Composites Part B: Engineering. 2017;114:101-10.

[15] Kong Q, Wu T, Zhang J, Wang D-Y. Simultaneously improving flame retardancy and dynamic mechanical properties of epoxy resin nanocomposites through layered copper phenylphosphate. Compos Sci Technol. 2018;154:136-44.

[16] Guan Q, Yuan L, Zhang Y, Gu A, Liang G. Improving the mechanical, thermal, dielectric and flame retardancy properties of cyanate ester with the encapsulated epoxy resin-penetrated aligned carbon nanotube bundle. Composites Part B: Engineering. 2017;123:81-91.

[17] Schartel B, Weiß A, Sturm H, Kleemeier M, Hartwig A, Vogt C, et al. Layered silicate epoxy nanocomposites: formation of the inorganic□carbonaceous fire protection layer. Polym Advan Technol. 2011;22(12):1581-92.

[18] Gao Y, Wu J, Wang Q, Wilkie CA, O'Hare D. Flame retardant polymer/layered double hydroxide nanocomposites. Journal of Materials Chemistry A. 2014;2(29):10996-1016.

[19] Nyambo C, Songtipya P, Manias E, Jimenez-Gasco MM, Wilkie CA. Effect of MgAl-layered double hydroxide exchanged with linear alkyl carboxylates on fire-retardancy of PMMA and PS. J Mater Chem. 2008;18(40):4827-38.

[20] Kalali EN, Wang X, Wang D-Y. Functionalized layered double hydroxide-based epoxy nanocomposites with improved flame retardancy and mechanical properties. Journal of Materials Chemistry A. 2015;3(13):6819-26.

[21] Wang X, Kalali EN, Wang D-Y. Renewable Cardanol-Based Surfactant Modified Layered Double Hydroxide as a Flame Retardant for Epoxy Resin. ACS Sustainable Chemistry & Engineering. 2015;3(12):3281-90.

[22] Kalali EN, Wang X, Wang D-Y. Multifunctional intercalation in layered double hydroxide: toward multifunctional nanohybrids for epoxy resin. Journal of Materials Chemistry A. 2016;4(6):2147-57.

[23] Li Z, Wang D-Y. Nano-architectured mesoporous silica decorated with ultrafine Co_3O_4 toward an efficient way to delaying ignition and improving fire retardancy of polystyrene. Mater Design. 2017;129:69-81.

[24] Qian Y, Wei P, Jiang P, Hao J, Du J. Preparation of hybrid phosphamide containing polysilsesquioxane and its effect on flame retardancy and mechanical properties of polypropylene composites. Composites Part B: Engineering. 2013;45(1):1541-7.

[25] Wang D-Y, Costa FR, Vyalikh A, Leuteritz A, Scheler U, Jehnichen D, et al. One-step synthesis of organic LDH and its comparison with regeneration and anion exchange method. Chem Mater. 2009;21(19):4490-7.

[26] Qian Y, Wei P, Jiang P, Li Z, Yan Y, Liu J. Preparation of a novel PEG composite with halogen-free flame retardant supporting matrix for thermal energy storage application. Appl Energ. 2013;106:321-7.

[27] Zhao X, Lu G, Whittaker A, Millar G, Zhu H. Comprehensive study of surface chemistry of MCM-41 using 29Si CP/MAS NMR, FTIR, pyridine-TPD, and TGA. The Journal of Physical Chemistry B. 1997;101(33):6525-31.

[28] Shao D, Jiang Z, Wang X. SDBS Modified XC□72 Carbon for the Removal of Pb (II) from Aqueous Solutions. Plasma Processes and Polymers. 2010;7(7):552-60.

[29] Li Z, Zhang J, Dufosse F, Wang D-Y. Ultrafine nickel nanocatalyst-engineering of an organic layered double hydroxide towards a super-efficient fire-safe epoxy resin via interfacial catalysis. Journal of Materials Chemistry A. 2018;6(18):8488-98.

[30] Li Z, Wang J, Expósito DF, Zhang J, Fu C, Shi D, et al. High-performance carrageenan film based on carrageenan intercalated layered double hydroxide with enhanced properties: Fire safety, thermal stability and barrier effect. Composites Communications. 2018;9:1-5.

[31] Abenojar J, Tutor J, Ballesteros Y, del Real J, Martínez M. Erosion-wear, mechanical and thermal properties of silica filled epoxy nanocomposites. Composites Part B: Engineering. 2017;120:42-53.

[32] Liu Y-L, Wei W-L, Hsu K-Y, Ho W-H. Thermal stability of epoxy-silica hybrid materials by thermogravimetric analysis. Thermochim Acta. 2004;412(1):139-47.

[33] Wang N, Zhang J, Fang Q, Hui D. Influence of mesoporous fillers with PP-g-MA on flammability and tensile behavior of polypropylene composites. Composites Part B: Engineering. 2013;44(1):467-71.

[34] Wang Y, Zhang J. Influences of specimen size and heating mode on the ignitability of polymeric materials in typical small□scale fire test conditions. Fire Mater. 2012;36(3):231-40.

[35] Chen Y, Zhan J, Zhang P, Nie S, Lu H, Song L, et al. Preparation of intumescent flame retardant poly (butylene succinate) using fumed silica as synergistic agent. Ind Eng Chem Res. 2010;49(17):8200-8.

[36] Menchi A, Scian A. Mechanism of cordierite formation obtained by the sol–gel technique. Mater Lett. 2005;59(21):2664-7.

[37] Ma HY, Tong LF, Xu ZB, Fang ZP. Functionalizing carbon nanotubes by grafting on intumescent flame retardant: nanocomposite synthesis, morphology, rheology, and flammability. Adv Funct Mater. 2008;18(3):414-21.

[38] Bourbigot S, Le Bras M, Delobel R. Carbonization mechanisms resulting from intumescence association with the ammonium polyphosphate-pentaerythritol fire retardant system. Carbon. 1993;31(8):1219-30.

[39] Matykiewicz D, Przybyszewski B, Stanik R, Czulak A. Modification of glass reinforced epoxy composites by ammonium polyphosphate (APP) and melamine polyphosphate (PNA) during the resin powder molding process. Composites Part B: Engineering. 2017;108:224-31.

[40] Liu Y-L, Hsu C-Y, Wei W-L, Jeng R-J. Preparation and thermal properties of epoxy-silica nanocomposites from nanoscale colloidal silica. Polymer. 2003;44(18):5159-67.

[41] Ke Z, Shi D, Yin J, Li RK, Mai Y-W. Facile method of preparing supertough polyamide 6 with low rubber content. Macromolecules. 2008;41(20):7264-7.

[42] Ren X, Tu Z, Wang J, Jiang T, Yang Y, Shi D, et al. Critical rubber layer thickness of core-shell particles with a rigid core and a soft shell for toughening of epoxy resins without loss of elastic modulus and strength. Compos Sci Technol. 2017;153:253-60.

Highlights

1. Layered double hydroxide (LDH) was engineered by silica via electrostatic induction

2. The targeted LDH-DBS@silica-1 formed intercalation structure in epoxy resin matrix

3. Fire safety was remarkably improved with 3wt% LDH-DBS@silica-1 to EP matrix

4. Glass transition temperature was increased after silica engineering on LDH-DBS

5. Impact strength was enhanced with silica engineering due to more craze initiation